Sensors and Materials, Vol. 36, No. 8 (2024) 3453–3463
MYU Tokyo

S & M 3744

Molecular Dynamics Analysis of Impact of Alloyed Interlayers in Ni–Al Reactive Multilayer Nanofoils

Rahul Kshetri, Mugilgeethan Vijendran, Takahiro Namazu, and Ryosuke Matsumoto*

Kyoto University of Advanced Science, 18 Yamanouchi Gotanda-cho, Ukyo-ku, Kyoto 615-8577, Japan

(Received June 3, 2024; accepted July 5, 2024)

Keywords: nickel, aluminum, reactive multilayer, exothermic reaction, molecular dynamic simulations

Reactive multilayer nanofoils (RMNFs), comprised of alternating layers of metals such as nickel and aluminum, have emerged as a focal point of interest owing to their distinctive properties and versatile applications across semiconductor and micro-electromechanical systems. This nanoengineered material undergoes a self-contained exothermic reaction, initiated by a small external trigger delivering localized heat up to 1500 °C in fractions of a second. It can be a heat source material primarily used to make a bond between electric components by melting solders. However, the volume shrinkage during reaction causes void formation and microcracking in the reaction product, and it reduces the reliability of the bonding. In this study, we systematically investigate 11 different Ni–Al RMNFs, including multilayers with 0, 10, 30, 50, 70, and 90% alloyed regions (polycrystalline B2-NiAl or amorphous-NiAl) using molecular dynamic simulations. We found that samples with alloyed interlayers exhibit reduced reaction temperatures and volume shrinkage after the reaction. By controlling the thickness of the alloyed interlayers and structures, we can reduce the damage caused by volume shrinkage during the reaction while obtaining a sufficient reaction temperature.

1. Introduction

Reactive multilayer nanofoils (RMNFs) have emerged as a subject of considerable interest over the past decades owing to their distinctive properties and versatile applications across multiple domains.[1,2] RMNFs are generally made up of layers of two metals, for example, Ni and Al. The reactive metals are fabricated by vapor-depositing thousands of alternating nanoscale layers of Ni and Al, which are currently commercially available as free-standing foils (Nanofoils®).[3] RMNFs deliver energy in a controlled and precise manner for joining, energetics, and heating applications. When the reaction is triggered by a brief pulse of energy from electrical, optical, thermal, or mechanical sources, an RMNF undergoes an exothermic reaction, rapidly providing localized heat up to a temperature of 1500 °C in fractions of a second.[3] The heat produced enables the continuous reaction, leading to a self-sustaining rapid exothermic reaction.[4]

*Corresponding author: e-mail: matsumoto.ryosuke@kuas.ac.jp
https://doi.org/10.18494/SAM5166

ISSN 0914-4935

When RMNFs are used as the heat source to melt solders as new joining techniques, three properties are required for the reactive materials: (1) maximum energy density, (2) reactions to single-phase microstructures, and (3) reaction products with room-temperature ductility.[5] This combination is needed to create a mechanically reliable bond for microelectronics. The maximum reaction temperature can be obtained by preparing the samples with an atomic ratio of Ni:Al = 1:1, and this also ensures a single-phase reaction product.[6] The challenge of achieving reaction products with ductility at room temperature remains unresolved and requires attention. Experimentally, it was found that the presence of numerous cracks originating from the reaction start point in the Ni–Al layer, caused by a 12% volume shrinkage upon forming an intermetallic compound, adversely impacts the mechanical reliability of the joint.[4] Minimizing cracks in the reacted Ni–Al layer is the main challenge when using Ni/Al RMNFs for bonding.[7] Moreover, to make a bond, an RMNF should produce sufficient heat to melt a solder.[8]

Studies on RMNFs by molecular dynamics (MD) simulations began around the year 2010. This was primarily prompted by the development of a suitable force field for the Ni–Al system by Purja Pun and Mishin during that period.[9] The initial focus of MD simulations was on relatively small systems. Then, self-sustaining reactions by MD simulations have been widely performed. The Ni–Al system remains the major model for MD simulations to date while, as far as we know, only single studies were performed on Ti–Al or Ru–Al.[5,10] The studies of Ni–Al RMNFs using MD simulations have primarily focused on the detailed processes of self-sustaining reactions. Baras and Politano first investigated the reactivity, microstructural transformations, and transport properties of Ni–Al RMNFs using MD simulations.[11] Their research revealed that the reaction in Ni–Al RMNFs is governed by the mutual dissolution of Ni and Al into one another, followed by the formation of the B2-NiAl intermetallic phase. This finding aligns with the conclusions drawn by Cherukara *et al*.[12] Schwarz and Spolenak have recently investigated the effect of alloyed interlayers on the reaction propagation in Ni–Al RMNFs.[13] Their research showed that it was pivotal to include the alloyed interlayer into MD simulations when trying to reproduce experimental systems. In addition, they also found that the alloyed interlayer can be used as a design parameter to affect the reaction rate. Although numerous MD simulations have been carried out to investigate the reaction kinetics in Ni–Al RMNFs, the methods of enhancing the ductility or reducing the defect density and residual stress of the reaction product have not been explored to the best of our knowledge.

The main purpose of this study is to search for a new optimization parameter of RMNFs that can generate enough temperatures needed for joining applications and can reduce the volume shrinkage in reaction products. The heat generation and the volume shrinkage occur at the same time when two elements (Ni and Al) are mixed. To achieve our goal, we systematically investigated different samples with different volume fractions and structures (B2 or amorphous) of alloyed interlayers between Ni and Al layers by MD simulations.

2. Simulation Model and Methodology

MD simulations were performed using the Large-scale Atomic/Molecular Massively Parallel Simulator (LAMMPS) package.[14] To calculate the interatomic forces between the individual

atoms in the samples, the embedded-atom method (EAM) potential developed by Purja Pun and Mishin was implemented.[9] This interatomic potential can effectively reproduce both the Ni and Al phases, reveal the interdiffusion process, and display the intermetallic phases of Ni and Al when reacted.[9]

Initially, we considered a Ni–Al RMNF model without an alloyed region and with stoichiometric ratio 1 (multilayer model). The dimensions are 33.7, 5.2, and 17.0 nm along the *x*-, *y*-, and *z*-directions, respectively. The Ni and Al crystals have <100> along the *x*-, *y*-, and *z*-directions. The alloyed structures were prepared through the rapid heating and cooling of the multilayer model using MD simulations. Periodic boundary conditions (PBCs) were applied in all directions. The multilayer model was heated up to 2100 K for 4 ns running isothermal isobaric MD (NPT ensemble). Subsequently, the samples were cooled to room temperature (300 K) for 12 or 6 ns under NPT conditions. The former and latter produced a fully reacted polycrystalline B2-NiAl structure and an amorphous-NiAl structure, respectively. The amorphous-NiAl structure partially includes B2-NiAl grains.

Then, a Ni–Al RMNF model with alloyed interlayers with a differential volume fraction was fabricated. To add an alloyed interlayer, equal amounts of Ni and Al atoms were removed around the Ni–Al interfaces in the multilayer model and replaced by alloyed interlayers with an appropriate thickness. In this way, the size of all the models was kept almost constant. The stoichiometric ratio between Ni and Al atoms was always chosen to be as close to 1 as possible. We employed eleven models in total, namely, one Ni–Al RMNF without alloyed interlayers, five Ni–Al RMNFs with B2-NiAl alloyed interlayers, and five Ni–Al RMNFs with amorphous-NiAl alloyed interlayers: 0% alloyed region [Model 0, Fig. 1(a)], 10% alloyed region (Models 10-B2 and 10-a), 30% alloyed region [Models 30-B2 and 30-a, Fig. 1(b)], 50% alloyed region (Models 50-B2 and 50-a), 70% alloyed region [Models 70-B2 and 70-a, Fig. 1(c)], and 90% alloyed region (Models 90-B2 and 90-a). All the models consist of ~230000 atoms.

After the models were created, the PBCs were imposed in the *y*- and *z*-directions with free faces at both ends of the system in the *x*-direction by introducing vacuum space. Then, they were initially equilibrated at a room temperature of 300 K by running the NPT ensemble for 0.5 ns. The ignition region (section A in Fig. 2) was designated along the left edge of the structure, where $x \leq 8.0$ nm (see Fig. 2). To ignite the self-propagating reaction, the region where $x \leq 8.0$ nm was heated to 2100 K, while all the atoms in the outer region (reaction region) were kept at 300 K. Subsequently, to observe the self-propagating reaction, the system was allowed to evolve in an NPH ensemble for 6 ns. Throughout the entire simulation, a time step of 2 fs was employed. The temperature damping parameter of 0.2 ps and the pressure damping parameter of 2 ps were respectively used for temperature and stress control. The scientific data visualization and analysis software OVITO[15] was used to visualize the interdiffusion process and crystal structures, and to evaluate the volume shrinkage.

3. Results and Discussion

The use of MD simulations for the study of reaction propagation in Ni–Al RMNFs has yielded three significant observations. The first observation pertains to the interdiffusion

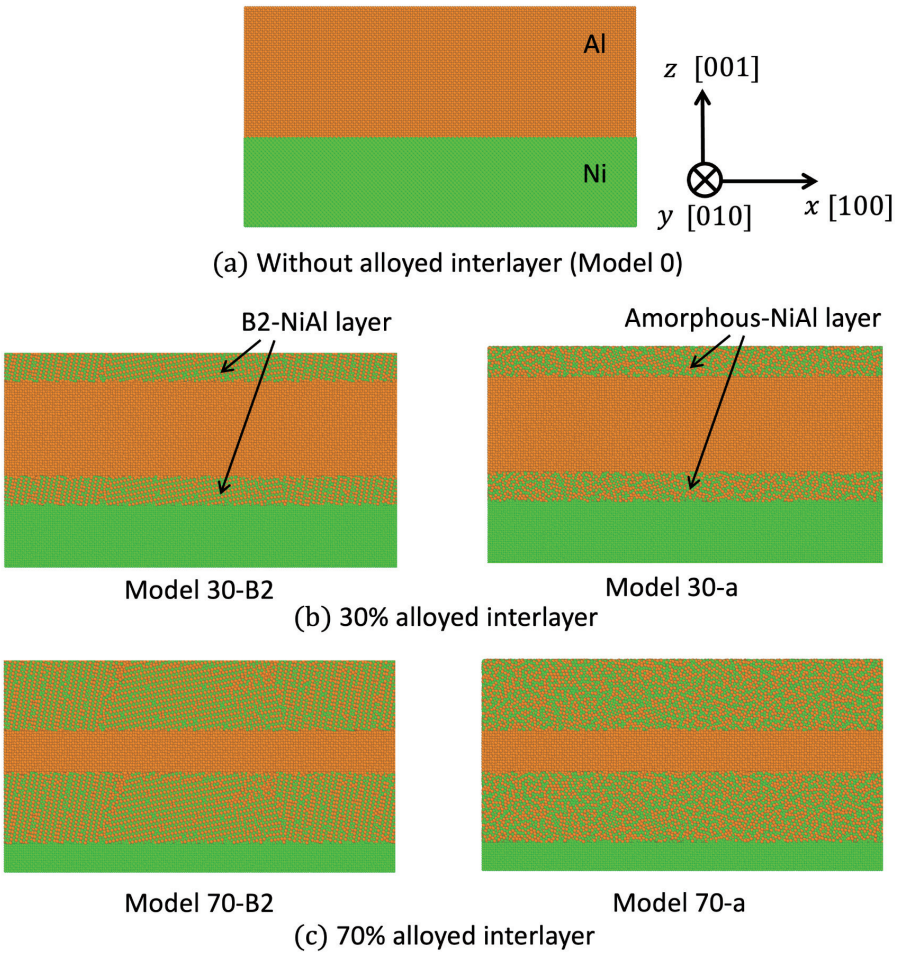

Fig. 1. (Color online) Simulation models presented with Ni atoms in green and Al atoms in orange.

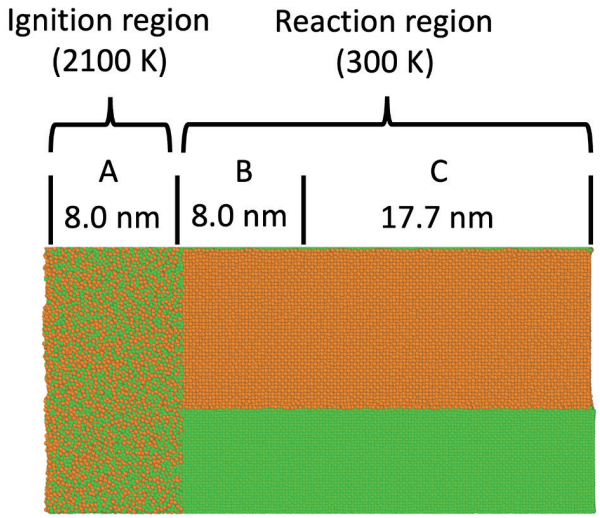

Fig. 2. (Color online) Ignition region being selected along the left edge of the structure, where $x \leq 8.0$ nm. In the figure, the ignition region was already melted by heating to 2100 K for Model 0.

process considering the RMNF without an alloyed interlayer (Model 0), the RMNFs with a 30% alloyed interlayer (Models 30-B2 and 30-a) , and the RMNF with a 90% amorphous-NiAl alloyed interlayer (Sect. 3.1). The second investigation compares the maximum reaction temperature reached during the reaction between the samples (Sect. 3.2). The third analysis assesses the impact of including alloyed interlayers between the Ni and Al layers on volume shrinkage after the completed reaction and quenching to 300 K (Sect. 3.3).

3.1 Reaction propagation in Ni–Al RMNFs

Figure 3 shows the reaction process observed in the RMNF without an alloyed interlayer (Model 0). As the heat propagates from the ignition region (Sect. A, initially 2100 K) to the reaction region (Sects. B and C, initially 300 K), the Al layer melts [right panel of Fig. 3(a)]. The Ni layer melts slower or does not melt since the melting point of Ni (~1728 K) is much higher than that of Al (~933 K).[16] The reaction started with the interdiffusion process where Ni atoms first diffused into molten Al [left panel of Fig. 3(a)]. The interdiffusion process continues [Fig. 3(b)] and Ni and Al are completely mixed [Fig. 3(c)]. During the reaction, the B2-NiAl phase nucleates and grows.

Figures 4 and 5 show the structures at 1 and 3 ns in the RMNFs with 30% of B2 and amorphous interlayers, respectively. After 3 ns, no significant change was confirmed. When B2-

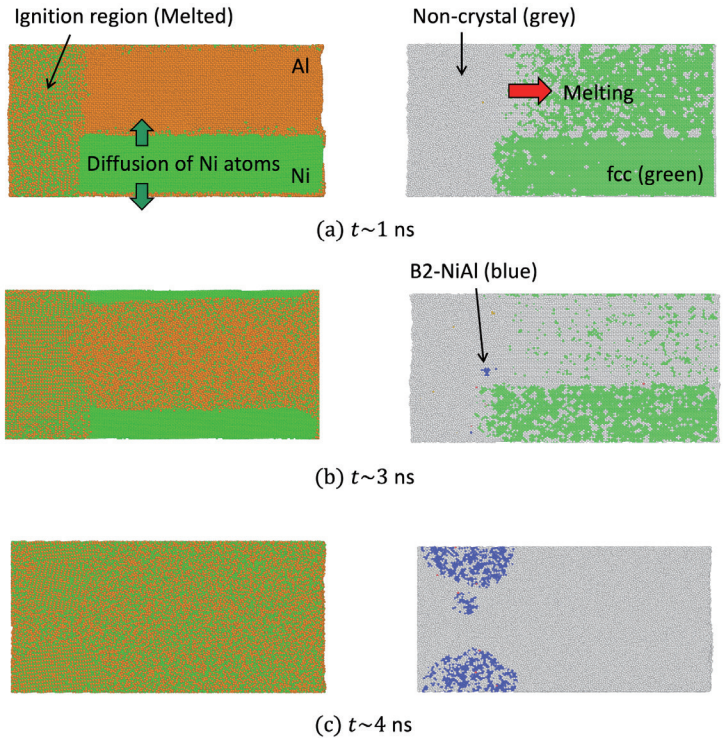

Fig. 3. (Color online) Ni–Al exothermic reaction of RMNF without alloyed interlayer (Model 0). Left panels show the distributions of Ni (green) and Al (orange) atoms. Right panels show the atomic structure based on the results of a common neighbor analysis where green, blue, red, and grey indicate fcc, bcc, hcp, and unidentified (i.e., liquid) structures, respectively.

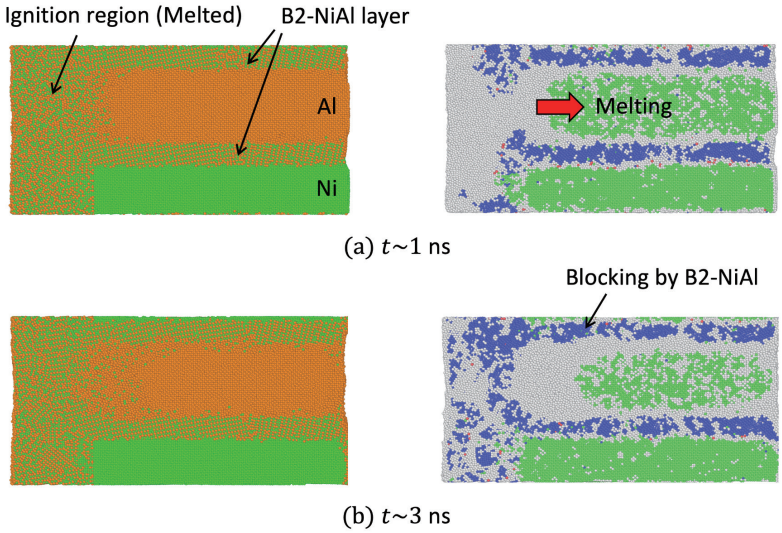

Fig. 4. (Color online) Ni–Al exothermic reaction for RMNF with 30% B2-NiAl alloyed interlayer (Model 30-B2).

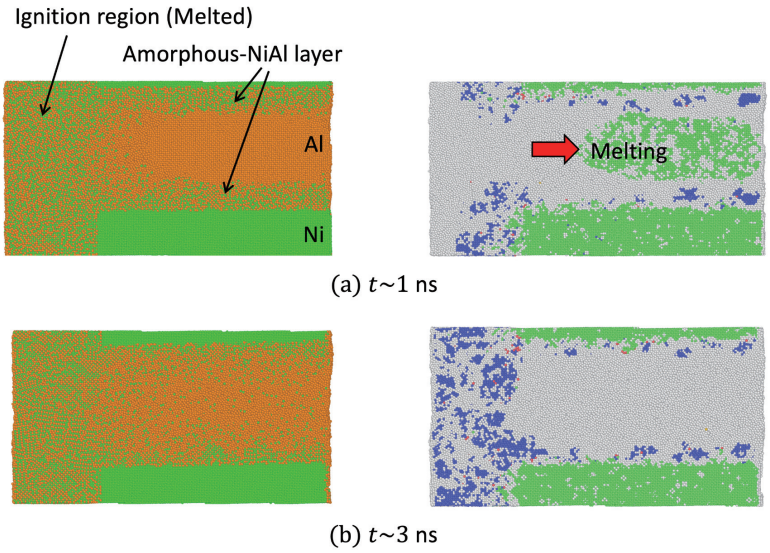

Fig. 5. (Color online) Ni–Al exothermic reaction for RMNF with 30% amorphous-NiAl alloyed interlayer (Model 30-a).

NiAl interlayers exist between the Al and Ni layers, the diffusion of Ni atom into molten Al is difficult since B2-NiAl has the highest melting point and intercepts the mixing (Fig. 4). Thus, most part of the Ni layer remains with the fcc structure [Fig. 4(b)]. We can confirm the migration of only a small amount of Ni atoms from the ignition region and the B2-NiAl layer to the melted Al layer [left panel of Fig. 4(b)]. On the other hand, when amorphous-NiAl interlayers exist, more intermixing occurs between the amorphous-NiAl and Al layers [Fig. 5(a)]. The amount of Ni atoms in the Al layer is more than that in the case with B2-NiAl [compare left panels of Figs. 4(b) and 5(b)], but it is less than that in the case without the alloyed interlayer [compare left panels of Figs. 3(b) and 5(b)]. Thus, a thin amorphous-NiAl layer also prevented the intermixing.

It was speculated that the B2-NiAl regions transformed from amorphous-NiAl intercepted the Ni migration. Figure 6 shows the structure change of the RMNF with the 90% amorphous alloyed interlayer (Model 90-a). We can clearly see the nucleation of many grains of B2-NiAl in amorphous-NiAl. The B2-NiAl grains gradually grow and cover almost all areas [Fig. 6(c)].

3.2 Temperature evolution during reaction

The temperature evolution within the RMNS without the alloyed layer (Model 0) is depicted in Fig. 7. After the ignition, heat is transferred from the ignition region (Sect. A) to the reaction region (Sects. B and C). Thus, the temperature of the ignition region (black curve) decreases and

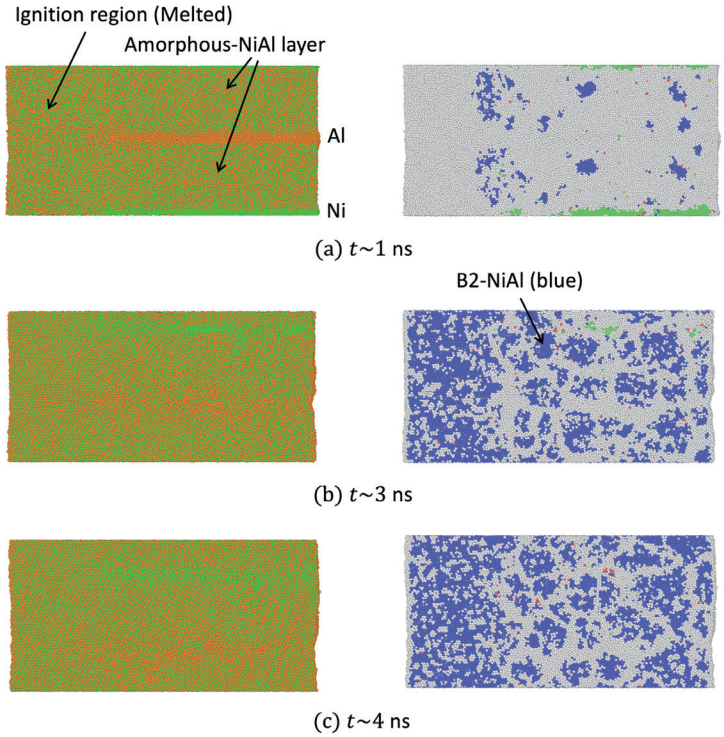

Fig. 6. (Color online) Ni–Al exothermic reaction for RMNF with 90% amorphous-NiAl alloyed interlayer (Model 90-a).

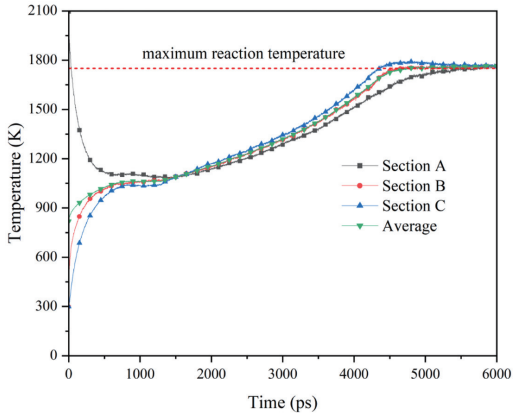

Fig. 7. (Color online) Plots of reaction temperature vs simulation time for the RMNF without alloyed interlayer (Model 0). The maximum reaction temperature is depicted by a red dashed line.

that of the reaction region (red and blue curves) increases. When intensive reaction is induced, the temperatures in Sects. B and C increase followed by the temperature increase in Sect. A. The temperature increase in Sect. A is caused by the heat conduction from the reaction region (Sect. B). The increase and saturation of the average temperature of the system (initially T^0_{ave} K, ≈ 727K, green curve) indicate the progress and completion (or suspension) of the reaction, respectively. The maximum reaction temperature T_{max} is determined by the saturation temperature as denoted by the red dashed line in Fig. 7, and it is obtained as ~1750 K.

Figure 8 shows the time evolution of the average temperature of the system of all the models. As discussed in the previous section, B2-NiAl intercepts the diffusion of Ni atoms from the Ni layer to melt the Al layer. The slight temperature increase observed in the models with B2-NiAl [Models 10-B2, 30-B2, 50-B2, 70-B2, and 90-B2; Fig. 8(a)] is caused by the mixing of molten NiAl in the ignition region and molten Al and the migration of Ni atoms in the B2-NiAl layer to molten Al as observed in Fig. 4(b). On the other hand, the slight temperature decrease [Fig. 8(a)] is caused by the energy consumption for the latent heat of melting of the Al layer. We can roughly evaluate the average heat generation (temperature increase) ΔT as a result of reactions in Sects. B and C as $\Delta T = (T_{max} - T^0_{ave}) \times L_x/L_{react}$, where L_x is the model size along x (33.7 nm) and L_{react} is the width of the reaction part (25.7 nm). We obtained $\Delta T \approx 1340$ K for Model 0. Similar

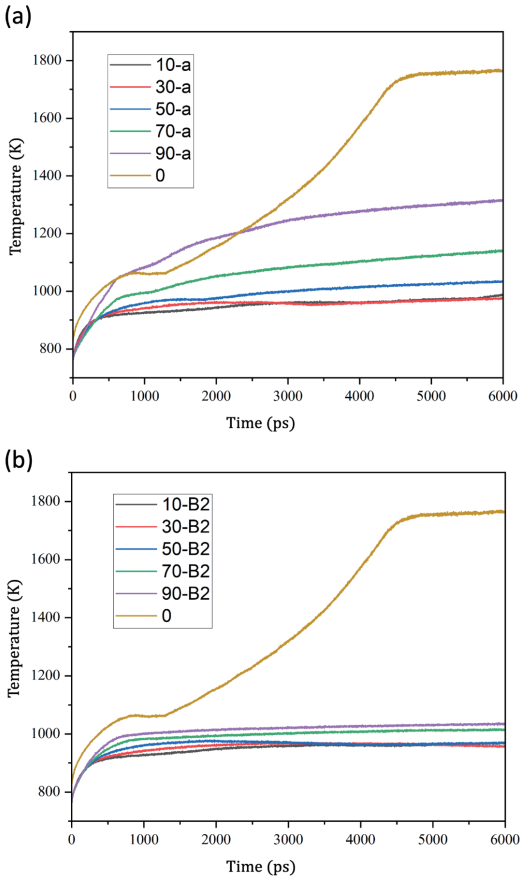

Fig. 8. (Color online) Comparison of the time evolution of average temperature of the system: (a) RMNFs with B2-NiAl alloyed interlayer and (b) RMNFs with amorphous-NiAl alloyed interlayer.

to Fig. 7, T_{max} and ΔT were evaluated for all models and are presented in Fig. 9. When amorphous layers were included, the reaction progressed slowly and was not completed during the simulation time (6 ns). We employed the final temperature of the system as T_{max}. The final temperature is expected to be slightly higher than the value shown in Fig. 9(b) especially at a higher volume fraction. When B2-NiAl alloyed interlayers were included, the heat generation was small. The reason why the heat generation becomes higher at higher volume fractions (Models 70-B2 and 90-B2) is unclear, but we speculate that the smaller volume of the Al layer reduced the heat consumption for the latent heat of melting. When amorphous-NiAl alloyed interlayers are used, we can confirm that as the volume fraction of the alloyed interlayer increases, the heat generation increases. Although the amorphous layers also prevent Ni diffusion from the Ni layer, as discussed in Fig. 5, the transformation of an amorphous structure to a B2 structure generates heat. The average-temperature increase in the reaction region ΔT is estimated to be >600 K except for the low volume fraction (Model 10-a). If those RMNFs are used to melt a SnAg solder for joining and the system is thermally isolated, they can melt approximately the same volume of SnAg solder since its melting point is 493 K.

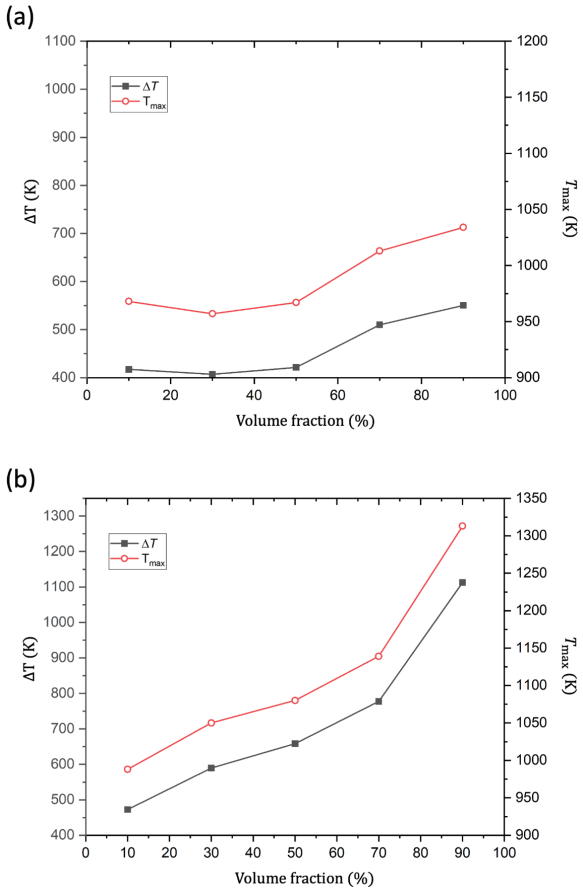

Fig. 9. (Color online) Reaction temperature and temperature rise of reaction region as a function of volume fraction of alloyed interlayer: (a) RMNFs with B2-NiAl alloyed interlayer and (b) RMNFs with amorphous-NiAl alloyed interlayer.

3.3 Volume shrinkage after the reaction

After an exothermic reaction in the Ni–Al RMNF with a 1:1 atomic ratio, the volume of the NiAl layer decreased by 12% owing to the reduced lattice spacing and a crystal structure shift from fcc to bcc.[1] After the simulation of the reaction presented in Sects. 3.1 and 3.2, the temperature for each model was first reduced to 300 K and the volumes were compared. The quenching of the crystal structure allowed for the formation of the bcc intermetallic compound (B2 structure). Figure 10 shows the typical structure after the quenching of the fully reacted system (Model 0), where the colors green, blue, red, and grey represent fcc, bcc, hcp, and unidentified structures, respectively.

Figure 11 shows the volume shrinkage from the initial structure at 300 K. The volume of the specimen was obtained using the construct surface mesh function of OVITO before (i.e., before ignition at 300 K) and after (i.e., after quenching at 300 K) the reaction. This surface mesh modifier identifies volumetric regions and allows the isolation of specific spatial regions enclosed by a surface and the calculation of their volumes.[15] The volume shrinkage in RMNFs with a B2-NiAl alloyed interlayer and RMNFs with a small volume of amorphous-NiAl alloyed interlayer is small. These results are reasonable because almost no reaction occurred. On the other hand, the volume shrinkage of RMNFs with a higher volume fraction of amorphous-NiAl (Models 70-a and 90-a) is relatively large, whereas it is still almost half of that of the RMNF

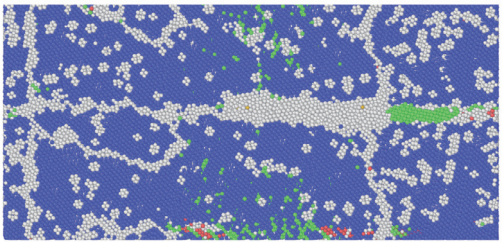

Fig. 10. (Color online) Atomic structure after the quenching of fully reacted system (Model 0).

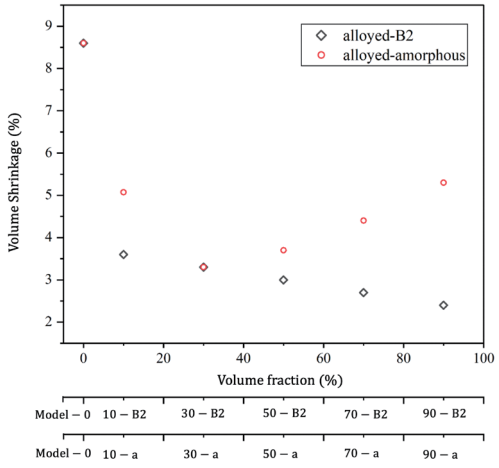

Fig. 11. (Color online) Volume shrinkage after the reaction.

without the alloyed interlayer (Model 0). The heat generation of Model 90-a is ~1100 K, which is comparable to that of Model 0 where $\Delta T \approx 1340$ K. Thus, a high volume fraction of the amorphous Ni–Al alloyed interlayer copes with both a high heat generation and a small volume shrinkage after the reaction.

4. Conclusion

We investigated the reaction temperatures and volume shrinkage for a RMNF without an alloyed interlayer and RMNFs with a differential thickness of alloyed interlayers. We found that the maximum reaction temperature and volume shrinkage decreased in the alloyed samples. When alloyed interlayers with the B2-NiAl structure were introduced, the reaction was terminated since the B2-NiAl layer intercepted the diffusion of Ni atoms from the Ni layer to the molten Al layer. The amorphous-NiAl alloyed layer also prevented the diffusion of Ni atoms from the Ni layer to the Al layer. However, the transformation of an amorphous structure to a B2 structure generated sufficient heat, whereas the volume shrinkage was also considerably reduced.

By controlling the thickness of the alloyed layer and its structure and atomic composition, we can reduce the damage caused by volume shrinkage during a reaction while obtaining a sufficient reaction temperature. Therefore, we have proposed the possible use of alloyed interlayers within RMNFs during fabrication tailored to desired applications.

References

1 S. Kanetsuki, T. Namazu, and S. Miyake: Sens. Mater. **31** (2019) 729. https://doi.org/10.18494/SAM.2019.2076
2 F. Baras, V. Turlo, O. Politano, S. G. Vadchenko, A. S. Rogachev, and A. S. Mukasyan: Adv. Eng. Mater. **20** (2018) 1800091. https://doi.org/10.1002/adem.201800091
3 Indium Corporation: https://www.indium.com/products/nanofoil/ (accessed April 1, 2024).
4 K. Maekawa, S. Ito, and T. Namazu: Jpn. J. Appl. Phys. **59** (2020) SIIL01. https://doi.org/10.35848/1347-4065/ab769b
5 K. Woll, A. Bergamaschi, K. Avchachov, F. Djurabekova, S. Gier, C. Pauly, P. Leibenguth, C. Wagner, K. Nordund, and F. Mücklich: Sci. Rep. **6** (2016) 19535. https://doi.org/10.1038/srep19535
6 T. Izumi, N. Kametani, S. Miyake, S. Kanetsuki, and T. Namazu: Adv. Exp. Mech. **4** (2019) 84. https://doi.org/10.11395/aem.4.0_84
7 K. Maekawa, K. Kodama, S. Miyake, and T. Namazu: Jpn. J. Appl. Phys. **60** (2021) SCCL15. https://doi.org/10.35848/1347-4065/abf39c
8 D. Yasugi, K. Kodama, D. Goto, M. Naito, and T. Namazu: J. Jpn. Soc. Exp. Mech. **22** (2022) 124. https://doi.org/10.11395/jjsem.22.124
9 G. P. Purja Pun and Y. Mishin: Philos. Mag. **89** (2009) 3245. https://doi.org/10.1080/14786430903258184
10 V. I. Jordan and I. V. Shmakov: J. Phys. Conf. Ser. **1281** (2019) 012030. https://doi.org/10.1088/1742-6596/1281/1/012030
11 F. Baras and O. Politano: Phys. Rev. B **84** (2011) 024113. https://doi.org/10.1103/PhysRevB.84.024113
12 M. J. Cherukara, K. G. Vishnu, and A. Strachan: Phys. Rev. B **86** (2012) 075470. https://doi.org/10.1103/PhysRevB.86.075470
13 F. Schwarz and R. Spolenak: J. Appl. Phys. **131** (2022) 075107. https://doi.org/10.1063/5.0079035
14 S. Plimpton: J. Comput. Phys. **117** (1995) 1. https://doi.org/10.1006/jcph.1995.1039
15 A. Stukowski: Modell. Simul. Mater. Sci. Eng. **18** (2010) 015012. https://doi.org/10.1088/0965-0393/18/1/015012
16 W. D. Callister, and D. G. Rethwisch: Materials Science and Engineering: An introduction (Wiley, USA, 2014) 9th ed., Chap. 2.